

Machine Learning Approach for Solar Wind Categorization

Hui Li^{1,4}, **Chi Wang**^{1,4}, **Cui Tu**^{2,4}, and **Fei Xu**³

¹State Key Laboratory of Space Weather, National Space Science Center, CAS, Beijing, 100190, China.

²State Key Laboratory of Space Weather, National Space Science Center, CAS, Beijing, 100190, China.

³Physics Department, Nanjing University of Information Science and Technology, Nanjing, China.

⁴University of Chinese Academy of Sciences, Beijing, 100049, China.

Key Points:

- An eight-dimensional scheme for 4-type solar wind categorization is developed based on 10 supervised machine-learning classifiers.
- Machine learning approach significantly improves the classification accuracy by $\sim 10\%$ over existing manual schemes.
- Classification only depends on typical solar wind observations, such as $N_{\alpha}, N_p, B_T, V_p, T_p$.

Abstract

Solar wind classification is conducive to understand the physical processes ongoing at the Sun and solar wind evolution in the interplanetary space, and furthermore, it is helpful for early warning of space weather events. With rapid developments in the field of artificial intelligence, machine learning approaches are increasingly being used for pattern recognition. In this study, an approach from machine learning perspectives is developed to automatically classify the solar wind at 1 AU into four types: coronal-hole-origin, streamer-belt-origin, sector-reversal-region-origin, and ejecta. By exhaustive enumeration, an eight-dimensional scheme (B_T , N_P , T_P , V_P , $N_{\alpha P}$, T_{exp}/T_P , S_P , and M_f) is found to perform the best among 8191 combinations of 13 solar wind parameters. 10 popular supervised machine learning models, namely k Nearest Neighbors (KNN), Support Vector Machines with linear and Radial Basic Function kernels, Decision Tree, Random Forest, Adaptive Boosting, Neural Network, Gaussian Naive Bayes, Quadratic Discriminant Analysis, and Extreme Gradient Boosting, are applied to the labeled solar wind data sets. Among them, KNN classifier obtains the highest overall classification accuracy, 92.8%. It significantly improves the accuracy by 9.6% over existing manual schemes. No solar wind composition measurements are needed, permitting our classification scheme to be applied to most solar wind spacecraft data. Besides, two application examples indicate that solar wind classification is helpful for the risk evaluation of predicted magnetic storms and surface charging of geosynchronous spacecrafts.

1 Introduction

In 1959, the first solar wind observation was made by the Soviet satellite, *Luna 1*. Since then, decades of in-situ solar wind measurements have firmly established that the solar wind plasma comes from different origins, for example, the coronal hole, the streamer belt, and active regions. Xu & Borovsky [2015, and references therein] showed that the solar wind can generally be classified into three major types: coronal-hole-origin plasma, streamer-belt-origin plasma, and ejecta.

Coronal-hole-origin plasma (CHOP) is sometimes called the fast solar wind, which originates from the open field line regions of coronal holes, and typically exhibits speeds in excess of 600 km/s at 1 AU and beyond [Sheeley et al., 1976; McComas et al., 2008]. Statistically, CHOP tends to be homogeneous [Bame et al., 1977] with a high proton temperature

and low plasma density [Schwenn, 2006], and is dominated by outward propagating Alfvénic waves [Luttrell & Richter, 1988]. It exhibits a statistical non-adiabatic heating of the protons between 0.3 to 1.0 AU [Hellinger et al., 2011]. In addition, field-aligned relative drifts between the alphas and protons can frequently be found in CHOP, with a speed up to the local proton Alfvén speed [Marsch et al., 1982]. Moreover, the relative fluctuations of magnetic field and solar wind velocity are large in CHOP, about 24% and 19%, respectively. However, the corresponding Fourier spectral indices are -1.56 and -1.55 [Borovsky, 2012], which is more likely to Iroshnikov-Kraichnan's theory ($f^{-3/2}$). As proposed by Li et al. [2011], this further indicates that current sheets are rare in such kind of solar wind.

Streamer-belt-origin plasma (SBOP), also known as the slow solar wind, has a typical speed less than 400 km/s. Compared to CHOP, SBOP does not exhibit much Alfvénic fluctuation [Schwenn, 1990] but is highly structured [Bame et al., 1977] with a low proton temperature and high plasma density [Schwenn, 2006]. In addition, the alpha-proton relative drift is typically absent in SBOP [Asbridge et al., 1976], and the protons are closer to adiabatic [Eyni & Steinitz, 1978]. The relative fluctuations of magnetic field and solar wind velocity are small in SBOP, which are only 16% and 11%, respectively. Different from the situations in CHOP, both of the corresponding Fourier spectral indices obey Kolmogoroff's law ($f^{-5/3}$), giving -1.70 and -1.67, respectively [Borovsky, 2012]. This indicates that the solar wind may contain many current sheet structures [Li et al., 2011].

Recently, it is found that SBOP can be further divided into two subgroups according to whether there exists an interplanetary magnetic sector reversal [Antonucci et al., 2005; Schwenn, 2006]. One subgroup is referred to as streamer belt plasma (SBP) without sector reversals, and the other one is referred to as sector reversal region plasma (SRRP) with one sector reversal. The origin mechanism of SBP at the Sun is still a major unsolved problem in solar physics. There are two main mechanisms of SBP origination. One is the interchange magnetic reconnection of open field lines with closed streamer belt field lines [Fisk et al., 1999; Subramanian et al., 2010; Antiochos et al., 2011; Crooker et al., 2012]; the other one is from the edge of a coronal hole near a streamer belt [Wang & Sheeley, 1990; Arge et al., 2003]. SRRP is suggested to be emitted from the top of the helmet streamers [Gosling et al., 1981; Suess et al., 2009; Foulon et al., 2011]. Statistically, SBP and SRRP have different characteristics in the solar wind and subsequent effects on the geospace environments, which have been summarized by Borovsky & Denton [2013].

Another major category of solar wind plasma is the so called ejecta (EJECT), which are associated with solar transients such as interplanetary coronal mass ejections (ICMEs) and magnetic clouds (MCs) [Richardson et al., 2000; Zhao et al., 2009]. The origination of EJECT is the magnetic reconnection associated with the structures of streamer belts or active regions, which can impulsively emit plasma and make the magnetic field deviate from the Parker spiral [Borovsky, 2010]. The typical signatures of EJECT at 1 AU have been well summarized [see Zurbuchen & Richardson, 2006, and references therein], for example, enhanced and smoothly rotating magnetic field, low proton temperature and plasma β , extreme density decrease, enhanced density ratio between alpha and proton, abundance and charge state anomalies of heavy ion species, bidirectional strahl electron beams, cosmic ray depletion, and declining velocity. Different from the expansions of CHOP or SBOP in the two directions transverse to radially outward from the Sun, impulsive EJECT expands in all three directions as they propagate outward [Klein & Burlaga, 1982]. Recently, Li et al. [2016] performed a statistical survey on Alfvénic fluctuations inside ICMEs, finding that only 12.6% of EJECT are found to be Alfvénic, and such a percentage decays linearly in general as the radial distance increases. The relative fluctuations of magnetic field and solar wind velocity are medium in EJECT, 21% and 15%, respectively [Borovsky, 2012]. The Fourier spectral indices are close to -5/3 [Borovsky, 2012], and may decrease as the radial distance increases [Li et al., 2017].

The categorization of the solar wind into its origin is of great importance for solar and heliospheric physics studies. Firstly, the statistical properties of solar wind should be clarified by its type to make a more comprehensive understanding of solar wind. Secondly, dividing the solar wind observations at 1 AU according to their origins can lead to a better diagnosing of physical processes ongoing at the Sun [Mariani et al., 1983; Thieme et al., 1989, 1990; Matthaeus et al., 2007; Borovsky, 2008; Zastenker et al., 2014]. Thirdly, the geoeffectiveness (geomagnetic activity, specifically, magnetic storm and substorm) of solar wind from different origins differ considerably [e.g., Borovsky & Denton, 2006; Turner et al., 2009; Borovsky & Denton, 2013]. Such a categorization would be helpful for the early warnings of space weather. Note that, these differences are in statistical terms. For individual cases, the situations may be quite different and complicated.

Usually, the solar wind classification is done manually by experienced people. In the literature, several empirical categorization methodologies in different parameter space have been proposed. In a one-dimensional parameter space, the solar wind was usually separated

into “fast wind” or “slow wind” according to its speed, V_p [Arya & Freeman, 1991; Tu & Marsch, 1995; Feldman et al., 2005; Yordanova et al., 2009]. However, such a V_p scheme can only roughly divide the solar wind into CHOP and SBOP, but could not separate out EJECT, SBP, and SRRP. Moreover, the criterion of V_p is not unique. In 2014, another one-dimensional scheme based on the parameter P_{type} ($= 2 \log S_p - \log(C^{6+}C^{5+}) - \log(C^{7+}C^{6+})$) was proposed by Borovsky & Denton [2014]. As the understanding of ICMEs and MCs is getting better, many methodologies have been proposed to identify EJECT [see Zurbuchen & Richardson, 2006; Kunow et al., 2006, and references therein], and several catalogs of EJECT at 1 AU have been produced [e.g., Lepping et al., 2005; Jian et al., 2006; Richardson & Cane, 2010]. Recently, the composition measurements were used for solar wind classification. An algorithm in a two-dimensional parameter space, such as O^{7+}/O^{6+} and V_p , was constructed by Zurbuchen et al. [2002]; Zhao et al. [2009]; von Steiger et al. [2010]. Such a two-dimensional scheme is still not able to divide SBOP into SBP and SRRP. In addition, such a scheme is not generally available for most solar wind spacecrafts due to the lack of on-board ion composition instruments. Xu & Borovsky [2015] developed a three-parameter, four-plasma-type categorization scheme based on commonly used solar wind measurements, and obtained a good classification accuracy. In addition, an on-board solar wind classification algorithm was already applied in the *Genesis* spacecraft [Neugebauer et al., 2003; Reisenfeld et al., 2003]. Such a automatic method requires the measurement of bi-directional electron and historic solar wind classification results.

Although the traditional classification has significant improvements in recent decades, there remains some improvement room for the existing empirical categorization schemes. The multi-label classification is regarded as a typical task of machine learning. Recently, the performance of machine learning classification is getting much better as the rapid developments of artificial intelligence theory and techniques. Machine learning technique is becoming more and more popular and powerful in big-volume data analysis in space physics, which may offer a solution to improve the accuracy of solar wind classification. Camporeale et al. [2017] recently employed a machine learning technique, Gaussian Process, in a four-category solar wind classification, and obtained a median accuracy larger than 96% for all categories. However, the time resolutions of the variables they used are not uniform. For example, the temporal resolution is one day for sunspot number and solar radio flux (10.7 cm), but is one hour for the other five solar wind parameters and for the reference solar wind data

sets. Camporeale et al. [2017] did not demonstrate the reasonableness of such mixture of hourly averaged solar wind parameters and daily sampled parameters.

In this work, we will apply 10 popular supervised machine learning models to identify the solar wind plasma into four types (CHOP, SBP, SRRP, EJECT) based on typical solar wind observations with the same temporal resolution of 1 hour. In particular, we will identify the best parameter scheme from 8191 combinations of 13 parameters derived from typical solar wind observations, judged by the classification accuracy as high as possible.

2 Methodology

For conventional classifications of the solar wind plasma at 1 AU, reference solar wind data with known plasma types should be first collected. Then, empirical relationships are developed to describe the domains of different plasma in some parameter space. Generally, the human experience performs well in two/three-dimensional parameter space. For a multi-dimensional space, humans cannot easily derive the empirical relationships.

For supervised machine learning approaches, reference solar wind data with known plasma types are needed for training the classifier as well. Then, the discriminant rules would be developed automatically by machine learning classifiers. One of the advantages is that the discriminant rules can be easily obtained in a multi-dimensional space for the machine learning perspective. Usually, 75% (80%) of the reference solar wind data are used for training, and the remaining 25% (20%) used for testing, especially for the situation with the cases less than 10000.

2.1 Machine Learning Classifiers

Classification is regarded as one of the typical tasks carried out by so-called machine learning system. The classifier is a critically important part of machine learning toolkit. As the rapid development of machine learning technique, a large number of classification algorithms have been developed. In this study, we will apply 10 widely used classifiers [Cady, 2017] to perform solar wind categorization, namely k -nearest neighbors (KNN), linear support vector machines (LSVM), SVM with a kernel of Gaussian radial basis function (RBFSVM), Decision Trees (DT), Random Forests (RF), Adaptive Boosting (AdaBoost), Neural Network (NN), Gaussian Naive Bayes (GNB), Quadratic Discriminant Analysis (QDA), and eXtreme Gradient Boosting (XGBoost). Table 1 gives the references of these 10 clas-

Table 1. 10 machine learning classifiers used in this study.

Classifier	Abbreviation	Reference
k -nearest neighbors	KNN	Denoeux [1995]
linear support vector machine	LSVM	Fan et al. [2008]
SVM with Gaussian radial basis function kernel	RBFSVM	Buhmann [2003]
Decision Trees	DT	Breiman et al. [1984]
Random Forests	RF	Ho [1995]
Adaptive Boosting	AdaBoost	Zhu et al. [2009]
Neural Network	NN	Rojas [1996]
Gaussian Naive Bayes	GNB	Perez et al. [2006]
Quadratic Discriminant Analysis	QDA	Srivastava et al. [2007]
Extreme Gradient Boosting	XGBoost	Chen & Guestrin [2016]

sifiers for readers to get more details. All the classification algorithms are included in the Scikit-learn package, which is an open source machine learning library written in the Python programming language [Pedregosa et al., 2011]. In this work, we will use the Scikit-learn package to carry out solar wind classifications. The details of the Scikit-learn package can be found at <http://scikit-learn.org/stable/index.html>.

2.2 Reference Solar Wind data

For supervised machine learning, reference solar wind data sets with known types are needed to train the classifiers. We use the same data sets utilized in [Xu & Borovsky, 2015], and the solar wind plasma will be divided into four types: CHOP, SBP, SRRP and EJECT. The collection of reference CHOP comes from the ideal events used by Xu & Borovsky [2015]. They examined the solar wind speed V_p , the proton-specific entropy $S_p = T_p/N_p^{2/3}$, O^{7+}/O^{6+} , C^{6+}/C^{5+} and the characteristics of the interplanetary magnetic field to identify CHOP. The intervals of twenty-seven day repeating steady high-speed solar wind streams with long intervals (days) are regarded as CHOP. CHOP starts after the compression of the corotating interaction region (CIR) and ends before the onset of the trailing edge rarefaction. At the same time, they also excluded large jumps in S_p , O^{7+}/O^{6+} or C^{6+}/C^{5+} to make sure

CHOP were not contaminated with ejecta. A total of 3049 hours of CHOP identified by Xu & Borovsky [2015] are used here.

The collection of reference SBP comes from the pseudo-streamers during 2002-2008 identified by Borovsky & Denton [2013]. Looking earlier in time the plasma upstream of the CIR, they checked the preceding intervals of CHOP. If the preceding coronal hole was of the same magnetic sector as the coronal hole immediately following the CIR, and if no sector reversals occurred in the streamer belt origin plasma between the successive two coronal holes, then the streamer belt plasma was classified into SBP. A total of 2275 hours of SBP identified by Borovsky & Denton [2013] are used here.

The collection of reference SRRP also comes from the work done by Xu & Borovsky [2015]. They examined the electron strahl observation and found some broad regions where the electron strahl dropped out around magnetic sector reversals at 1 AU. They denoted the regions where the strahl was very weak, intermittent, and/or intermittently bi-direction just outside the strahl dropped out regions, to be “strahl confusion zones”. The solar wind from these confusion zones are defined as SRRP. A total of 1740 hours of SRRP are used here.

The magnetic cloud collection made by [Lepping et al., 2005] is used to represent EJECT here, which can be found at http://wind.gsfc.nasa.gov/mfi/mag_cloud_pub1.html. Magnetic clouds are believed to be a subset of interplanetary coronal mass ejections (ICMEs) with an enhancement of magnetic field intensity and a gradual rotation in direction. The typical properties of magnetic cloud are a flux rope field configuration, low proton temperatures and low plasma beta value [Klein & Burlaga, 1982]. In general, only about one third of ICMEs can be regarded as magnetic clouds [Bothmer & Schwenn, 1996; Richardson & Cane, 2004]. Xu & Borovsky [2015] found a dual-population structure for the collection of ICMEs identified by Richardson & Cane [2010], but a single population for the collection of magnetic clouds identified by Lepping et al. [2005]. They believed that magnetic clouds can better present ejecta from the Sun, while the collection of ICMEs probably contains some non-ejecta data. A total of 1926 hours of EJECT are used here.

After removing some data gaps, the reference data set is composed of 2881 (33.4%) 1-hr events categorized as CHOP, 2215 (25.7%) events of SBP, 1694 (19.6%) events of SRRP, and 1835 (21.3%) events of EJECT. The imbalance ratio of these four types solar wind may affect the classification accuracy. In general, the accuracy would be relatively low when fewer reference solar wind are used for training. The ratio of reference SRRP is the lowest.

Table 2. List of 13 parameters used for solar wind classification.

Parameter	Symbol
magnetic field intensity	B_T
proton density	N_p
proton temperature	T_p
solar wind speed	V_p
proton-specific entropy	S_p
Alfvén speed	V_A
temperature ratio	T_{exp}/T_p
ratio of proton and alpha number density	$N_{\alpha p}$
dynamic pressure	P_d
solar wind electric field	E_y
plasma beta value	β
Alfvén Mach number	M_A
fast magnetosonic Mach number	M_f

Its classification accuracy is indeed found to be lower than the other three types in the following section. The solar wind parameters used in this study are from the OMNI database (<http://omni.gsfc.nasa.gov/>), which is primarily a 1963-to-current compilation of hourly-averaged, near-Earth solar wind magnetic field and plasma parameter data from several space-crafts in geocentric or L1 (Lagrange point) orbits. The data have been extensively cross compared and cross-normalized for some space-crafts and parameters.

3 Categorization Results

With the input of solar wind parameters and information of solar wind types, the classifiers can build discriminant rules automatically based on machine learning algorithms. Note that, most solar wind space-crafts have no composition instrumentation. To make the applicability of our classification scheme more extensive, the typical solar wind observations (the magnetic field intensity, B_T , the proton number density, N_p , the alpha particle number density, N_{α} , the proton temperature, T_p , and the solar wind speed, V_p) and their derived quantities are used here. As listed in Table 2, a total of 13 parameters are used for so-

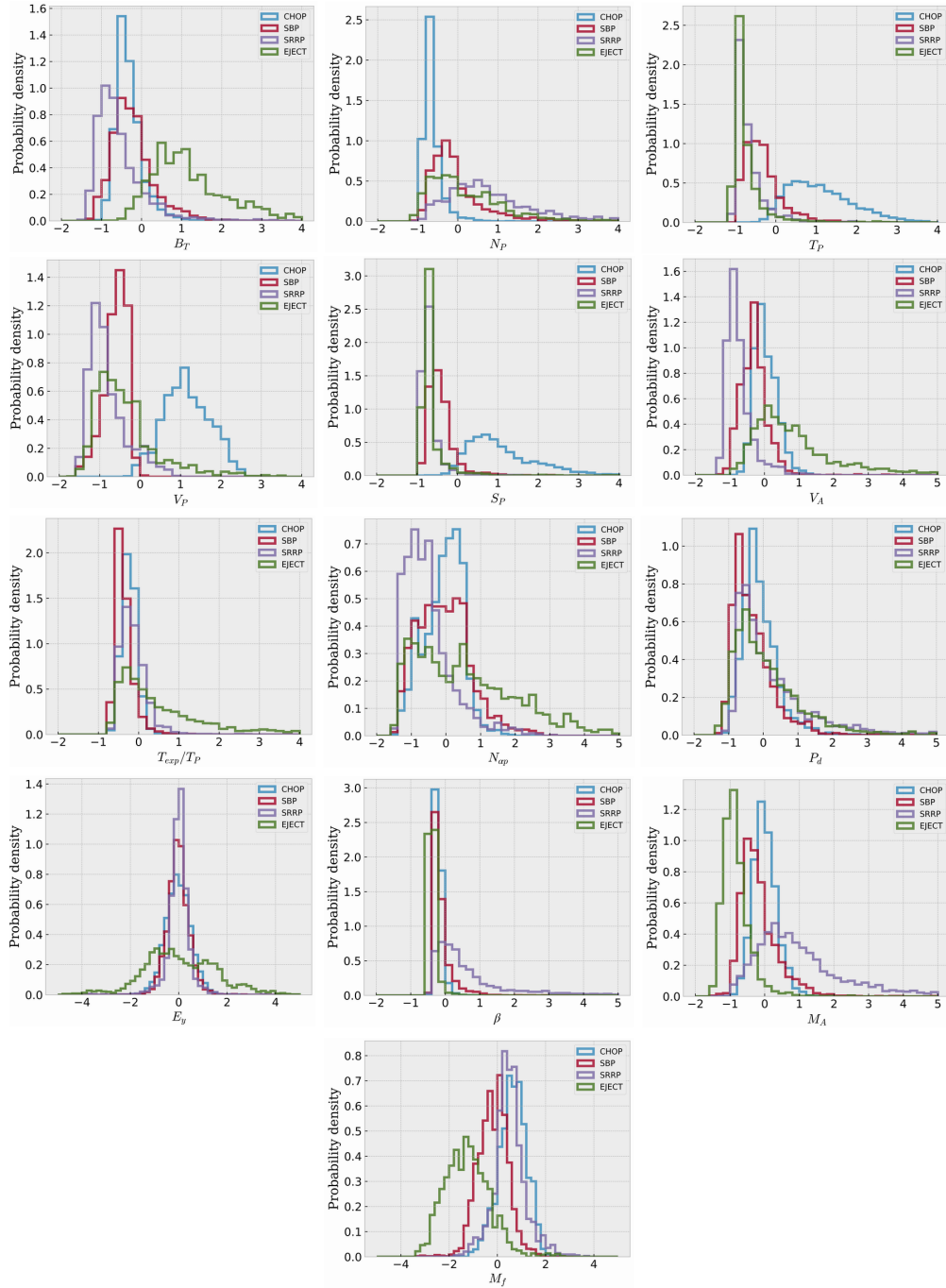


Figure 1. Probability density distributions of 13 solar wind parameters calculated from the whole reference solar wind data sets. The parameters have been rescaled as follows: $X = (X - \bar{X})/\sigma_X$. The area under each curve equals 1.

lar wind classification, such as B_T , N_p , T_p , V_p , the proton-specific entropy, S_p , the Alfvén speed, $V_A = B_T / \sqrt{\mu_0 m_p N_p}$ (μ_0 is the permeability in vacuum and m_p is the mass of proton), the temperature ratio, T_{exp}/T_p ($T_{exp} = (V_p/258)^{3.113}$ is the velocity-dependent expected proton temperature given by Xu & Borovsky [2015] in unit of eV), the number density ratio of proton and alpha, $N_{\alpha p}$, the dynamic pressure, P_d , the solar wind electric field, E_y , the plasma beta value β , the Alfvén Mach number, $M_A = V_A/V_p$, and the fast magneto-sonic Mach number, $M_f = V_p / \sqrt{C_s^2 + V_A^2}$ (C_s is the acoustic velocity). Note that, this parameter list includes all the parameters used in [Xu & Borovsky, 2015] and four of seven parameters used in [Camporeale et al., 2017]. As mentioned, the reference solar wind with known types is from hourly-averaged OMNI database, thus, only the parameters with a temporal resolution of one hour are considered here. The parameters with a temporal resolution of one day used in [Camporeale et al., 2017], the Sunspot number and solar radio flux (10.7 cm), are not considered here. Among them, a specific combination of parameter with the highest classification accuracy will be chosen for further analysis.

Figure 1 shows the probability density distributions of the above 13 parameters calculated from the whole reference solar wind data sets. Similar probability density distributions of V_p , V_A , S_p , and T_{exp}/T_p , are also shown by Camporeale et al. [2017]. Note that, the parameters have been rescaled as follows: $X = (X - \bar{X})/\sigma_X$, where \bar{X} represents the mean value of a parameter, and σ_X denotes the standard deviation. Obviously, it is difficult to distinguish the 4-type solar wind well from any individual probability distribution, which motivates the classification in a multi-dimensional space. Nevertheless, some parameters could contribute to distinguish some solar wind type from the others. For example, B_T and M_f contribute to distinguish EJECT from the others, especially from the SRRP; N_p , V_p , and $N_{\alpha p}$ are useful to distinguish between CHOP and SRRP; T_p and S_p help to distinguish CHOP from the others; and V_A is helpful to distinguish SRRP from the others. A natural thought is that the classification accuracy would be improved greatly by considering the above eight parameters together. Actually, the selected eight-dimensional parameter scheme with the best classification accuracy for KNN classifier contains 7 of the above 8 parameters, only with V_A replaced by T_{exp}/T_p .

Given 13 input features, a total of 8191 combinations exist. Taking the KNN classifier as an example, the classification accuracy is calculated by using all the 8191 combinations of input features. The eight-dimensional scheme, the combination of B_T , N_p , T_p , V_p , $N_{\alpha p}$, T_{exp}/T_p , S_p , and M_f is found to perform the best, with the overall accuracy of 92.8%.

Table 3. Classification performances for 10 classifiers based on the combination of B_T , N_p , T_p , V_p , $N_{\alpha p}$, T_{exp}/T_p , S_p , and M_f . From second to sixth column, the value gives the classification accuracy. The last column gives the Hanssen and Kuipers' Discriminant, HKSS. Note that, 75% of the reference solar wind data are used for training, and the remaining 25% used for testing. 100 iterations with random selection of the training data are run and the mean accuracies are reported here.

	CHOP	SBP	SRRP	EJECT	4-type	HKSS
KNN	99.2	91.1	83.8	92.9	92.8	0.902
XGBoost	99.2	90.9	83.6	92.8	92.6	0.898
RF	99.3	90.2	81.6	94.1	92.3	0.895
RBF SVM	99.1	89.0	81.1	94.1	91.9	0.890
NN	99.1	88.7	80.6	92.2	91.3	0.881
DT	98.1	84.8	77.6	89.0	88.7	0.846
LSVM	99.0	81.1	71.1	88.2	86.6	0.816
QDA	98.7	80.4	75.0	73.7	84.0	0.779
GNB	96.8	76.0	76.9	73.1	82.5	0.767
AdaBoost	97.5	85.1	45.2	85.6	81.5	0.737

The accuracy for classifying CHOP, SBP, SRRP, and EJECT is 99.2%, 91.1%, 83.8%, and 92.9%, respectively. Although this scheme is choosing from 8191 combinations of 13 variables from the perspective of practical effect, it really has physical meanings. As shown in Figure 1, these parameters indeed contribute to distinguish some solar wind type from the others. If some new variables are considered, another method to determine the variable combination may also work and reduce the test number greatly. For example, identify the first variable, by using that alone the best classification accuracy can be obtained. Then, identify the second variable, by considering that with the first determined variable together the best classification accuracy can be obtained. At last, repeat the second step until the accuracy could not be improved by adding any new variable. Actually, a set of mutually independent variables contain enough information of the classification system. Here, some combined parameters, e.g., S_p , V_A , T_{exp}/T_p , etc, are used only for the perspective of improving the classification accuracy. If the mutually independent variables (B_T - V_p - N_p - T_p - N_{ap}) are used, the classification accuracy of 4-type solar wind will decline slightly from 92.8% to 92.0%.

The classification is also done for the other 9 classifiers with the same parameter scheme used. The results are listed in Table 3. Five classifiers, KNN, XGBoost, RF, RBFSVM, and NN, produce the accuracy better than 90%. DT and LSVM also perform well, with the overall accuracy better than 85%. The remaining classifiers, QDA, GNB, and AdaBoost, yield accuracies between 80-85%. It should be mentioned that the overall accuracy for the other 9 classifiers should be improved if some special kind of parameter combination were used. The identification of CHOP is relatively easy. All the 10 classifiers work very well, with the accuracy better than 96.5% and the highest accuracy given by RF of 99.3%. For identifying EJECT, the accuracy decreases slightly. Only 5 classifiers yield accuracies better than 92%, and the highest accuracy given by RBFSVM is 94.1%. For identifying SBP, only 3 classifiers yield accuracies better than 90%, with the highest accuracy given by KNN of 91.1%. The identification of SRRP is relatively difficult. Only 5 classifiers yield accuracies better than 80%, and the highest accuracy given by KNN is only 83.8%. Note that, 75% of the reference solar wind data are used for training, and the remaining 25% used for testing. To make sure that our results are independent on the choice of training data set, cross validation is quite necessary. Thus, we perform 100 runs with the training data set being chosen randomly. The accuracy given in Table 3 is the averaged value of the 100 tests.

Besides the classification accuracy, the Hanssen and Kuipers' Discriminant, HKSS, is also given in Table 3. The HKSS, also known as the True Skill Statistic, represents the

classification accuracy relative to that of random chance. For multi-category classification, its expression can be written as follows:

$$HKSS = \frac{\frac{1}{N} \sum_{i=1}^K n(F_i, O_i) - \frac{1}{N^2} \sum_{i=1}^K N(F_i)N(O_i)}{1 - \sum_{i=1}^K (N(O_i))^2} \quad (1)$$

where $n(F_i, O_i)$ denotes the number of classifications in category i that had observations in category i , $N(F_i)$ denotes the total number of classifications in category i , $N(O_i)$ denotes the total number of observations in category i , and N is the total number of classification. HKSS ranges from -1 to 1. 1 represents the perfect performance, 0 denotes no improvement over a reference classification, and ≤ 0 indicates worse than the reference. From Table 3, it is clear that the results of HKSS for 10 classifiers are similar with the results of accuracy.

To test the sensitivity of variable in our eight-dimensional scheme, one variable is in turn left out from the scheme and the accuracies are recalculated accordingly. When S_p is not considered, the classification accuracy has the least decrease, 0.1%. And the accuracy has the largest decrease, 2.2%, when $N_{\alpha p}$ is not considered. However, it does not imply that S_p is the least importance variable in solar wind classification. Actually, the highest classification accuracy is obtained by using S_p alone, among the 13 variables. For different parameter combination, the most sensitive parameter should be different as well.

It is hard to make sure that the result of supervised machine learning is neither over-fitted nor under-fitted. Comparing the accuracy of training vs. testing data sets is a good way, but not sufficient. Cross validation is another strategy to overcome such problems. Following the methodology of Camporeale et al. [2017], we also compare the results of 100 runs for different ratios of the training data. In general, over-fitting is especially likely in cases where training examples are rare. Thus, a relative large ratio of training data, for example, 45%, 60%, 75%, and 90% are used, and the results are shown in Figure 2. The boxes denote the first and third quartiles of the accuracy distribution. The horizontal lines and triangles represent the median and mean values, respectively. The whiskers denote the 2nd and 98th percentiles. It is clear that the mean accuracy slightly increases when the ratio of training data increases from 45% to 75%. For the ratio of 90%, the accuracy has no significant improvement, however, the variation amplitude of classification accuracy increases significantly, and the lowest accuracy even decreases slightly for identifying SBP, SRRP, and EJECT. In the following texts, the accuracies are all obtained by using 75% of the data for training. This is just a simple approach to judge whether an over-fitting occurs or not. There may exist other, more robust, means of examining over-fitting or under-fitting. Camporeale et al. [2017]

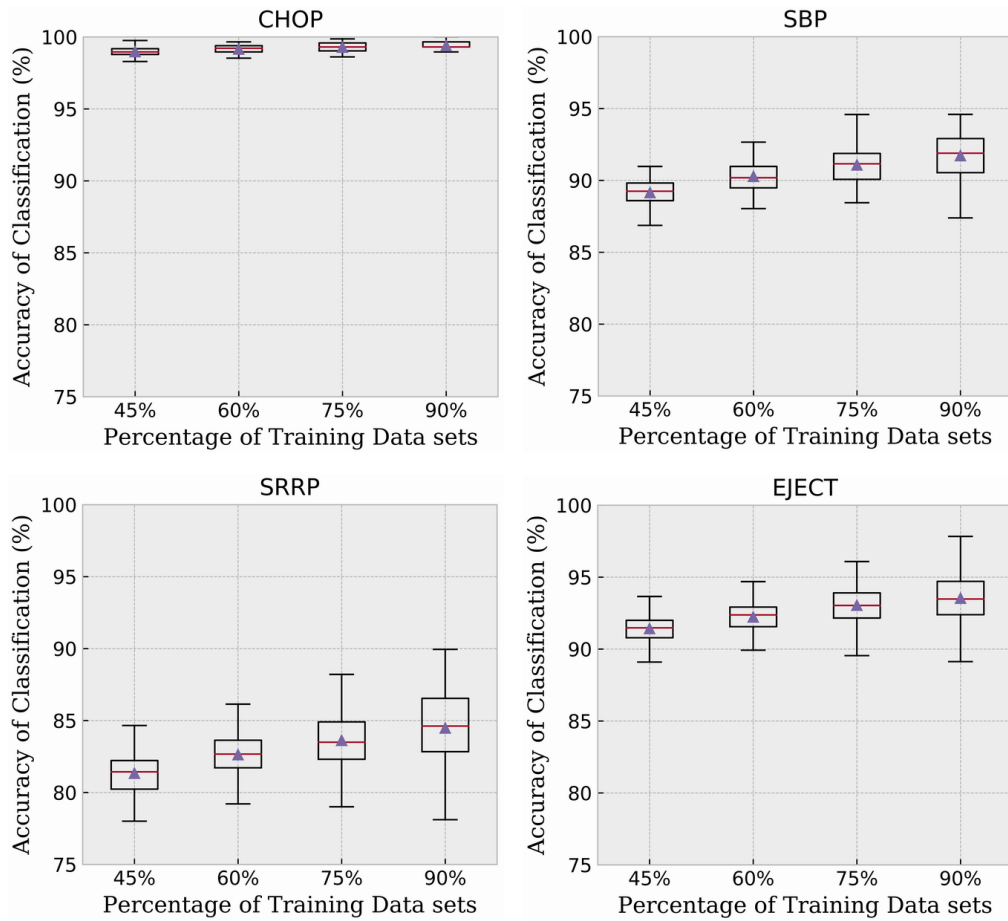


Figure 2. Accuracy of the KNN classifier calculated from 100 runs with different ratio of training data set being chosen randomly. The boxes denote the first and third quartiles of the accuracy distribution. The horizontal lines and triangles represent the median and mean values, respectively. The whiskers denote the 2nd and 98th percentiles.

showed the accuracy of the Gaussian Process classification model with 10%, 15%, 20%, and 25% of the original data used for training. Similarly, the accuracy increases when more data is used for training.

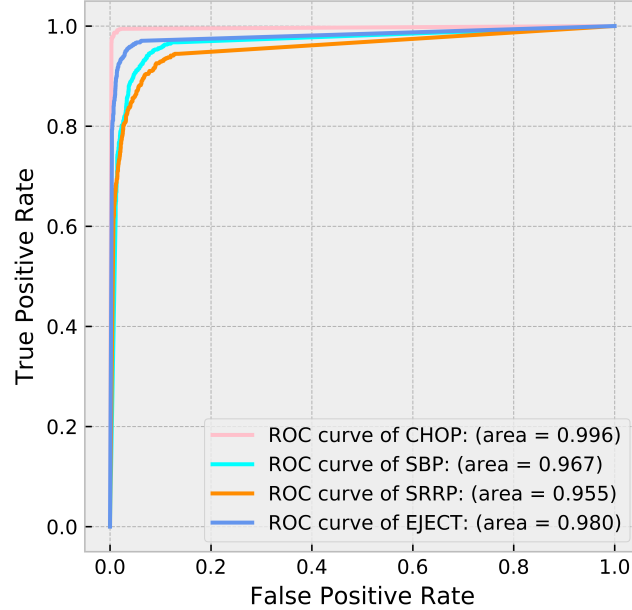


Figure 3. Receiver operating characteristic (ROC) curves for CHOP, SBP, SRRP, and EJECT. The False Positive Rate is defined as the ratio of false positives divided by the total number of negatives. The True Positive Rate denotes the ratio of true positives divided by the total numbers of positives. The area of the curve represents the goodness of binary classification, and unity denotes the perfect result.

For binary classification, the threshold of probability changes to accuracy in terms of true and false positives and negatives. Here, “true/false” denotes correct, or incorrect, classification, and “positive/negative” denotes that the solar wind is classified to be, not to be, some type. Thus, “true positive/false positive” denotes that the solar wind is correctly/incorrectly classified to be some type, while “true negative/false negative” denotes that the solar wind is correctly/incorrectly classified not to be some type. The Receiver operating characteristic (ROC) curve for different values of thresholds gives a concise representation of this metric. The horizontal axis is the False Positive Rate (FPR), which is defined as the ratio of false positives divided by the total number of negatives. And the vertical axis is the True Positive Rate (TPR), which denotes the ratio of true positives divided by the total numbers of positives. A perfect classification would give $FPR = 0$, $TPR = 1$, and the area of ROC curve equals unity. Figure 3 shows the ROC curves for CHOP, SBP, SRRP, and EJECT. The areas

of the curves are 0.996, 0.967, 0.955, and 0.980, respectively, indicating that the classification is pretty good. From practice, the threshold of probability can be chosen to be 0.3-0.5 to obtain optimal FPR and TPR, which is consistent with Camporeale et al. [2017].

Figure 4 shows an example of solar wind classification obtained by the KNN classifier. The shaded regions represent the time intervals of reference solar wind with known types. In general, all the solar wind can be distinguished well. It is clear that the CHOP, SBP, and EJECT in the shaded regions are identified perfectly with the accuracy nearly 100%. The classification accuracy for SRRP is not so high but still good, $\sim 85\%$. Occasionally, it is wrongly identified as SBP (on April 19, 28-29, and May 5) or CHOP (on May 13). Two long-duration EJECTs are also identified after CHOPs, for example, the EJECT on May 15-17, and 20, which had already been identified as two magnetic clouds by [Lepping et al., 2005]. At the same time, some short-duration EJECTs (several hours) are also identified on May 09-10 and 30-31, which may be the so-called small flux ropes proposed by Moldwin et al. [2000], and are in agreement with the small-scale magnetic flux rope database (<http://fluxrope.info/>) given by Dr. Jinlei Zheng and Dr. Qiang Hu at University of Alabama Huntsville. This indicates that our categorization scheme may in certain cases be useful for identifying small flux ropes, but more investigation and validation is needed.

Table 4 gives the comparison of the performances of various categorization schemes. The $O^{7+}/O^{6+}-V_p$ scheme proposed by Zhao et al. [2009] can not distinguish SBP and SRRP, and does not work well for identifying EJECT. The accuracy is only 63.5%. Xu & Borovsky [2015] proposed the $S_p-V_A-T_{exp}/T_p$ scheme, which has a significant improvement on identifying EJECT and increases the accuracy to 87.5%. In addition, such a scheme can also distinguish SBP and SRRP, with an accuracy $\sim 70\%$. Note that, the classification accuracies obtained by Xu & Borovsky [2015] are quite comparable to those obtained by KNN classifier. By taking the advantage of machine learning on classification in multi-dimensional parameter space, we apply an eight-dimensional scheme, the $B_T-N_P-T_P-V_P-N_{ap}-T_{exp}/T_P-S_p-M_f$ scheme, on KNN classifier, and obtain significant improvements in classification accuracies. The improvements of accuracy for identifying CHOP, SBP, SRRP, and EJECT is 2.3%, 21.2%, 11.8%, and 5.4%, respectively. For the 4-type solar wind classification, the overall accuracy has an improvement of 9.6%. It should be mentioned that, the feature space has been optimized only for the KNN approach. For other classifiers with some other parameter scheme used, the accuracies could be improved. Camporeale et al. [2017] proposed a classification scheme based on Gaussian Process classifier. By using the $V_p-\sigma_T-SSN-F10.7-V_A-$

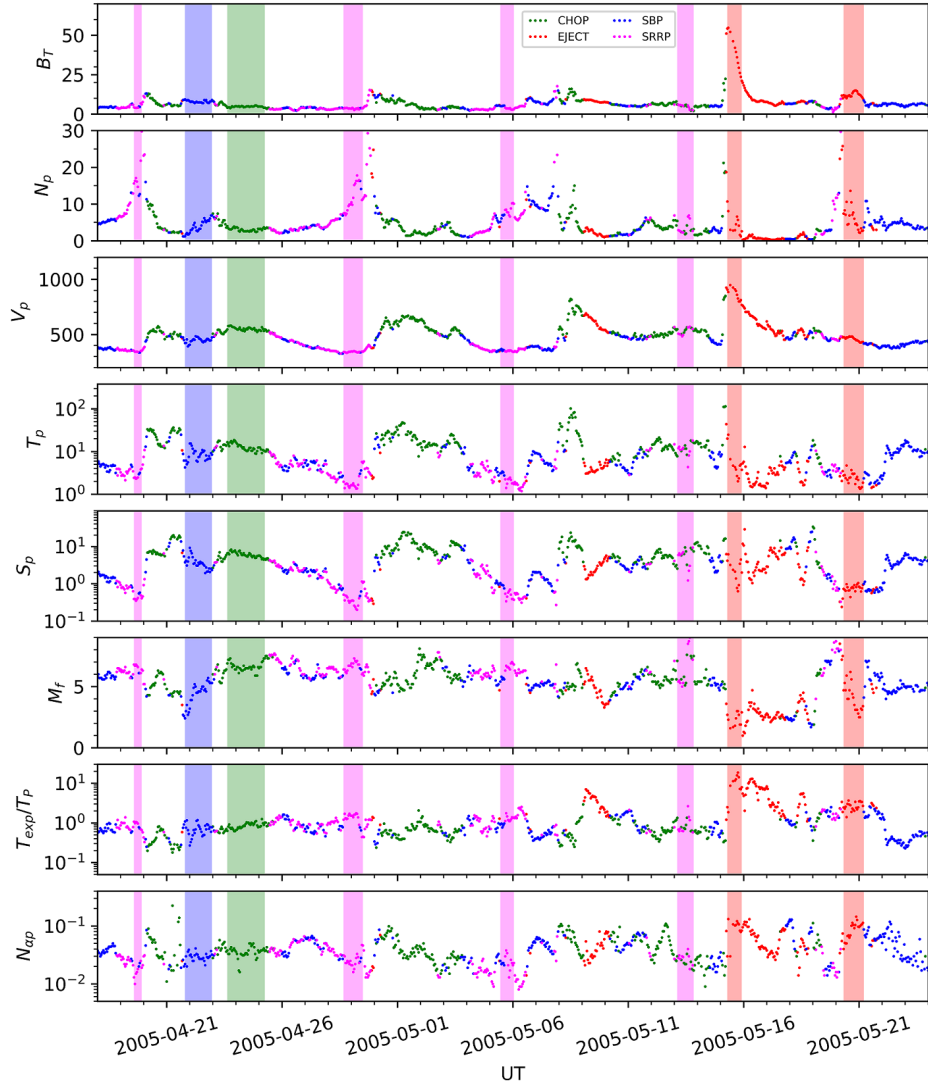


Figure 4. An example of solar wind classification obtained by the KNN classifier. From top to bottom, the panel represents the magnetic field intensity, the proton number density, the solar wind speed, the proton temperature, the proton-specific entropy, the plasma beta value, the fast magneto-sonic Mach number, the dynamic pressure, and the ratio of proton and alpha number density. The units are in nT, cm^{-3} , km/s, eV, eVcm^2 , unity, unity, nPa, and unity, respectively. The shaded regions represent the time intervals of reference solar wind with known types.

Table 4. Accuracies of various categorization schemes in solar wind classification. Note that, 25% of the database is used for training in [Camporeale et al., 2017], but the ratio is 75% in our study. 100 iterations with random selection of the training data are run and the mean accuracies are reported here.

Accuracy (%)	CHOP	SBP	SRRP	EJECT	4-type
$O^{7+}/O^{6+}-V_p$ Zhao et al. [2009]	98.0	73.0		63.5	
$S_p-V_A-T_{ex}/T_p$ Xu & Borovsky [2015]	96.9	69.9	72.0	87.5	83.2
$S_p-V_A-T_{exp}/T_p$ KNN (this work)	97.2	74.9	69.7	88.7	84.3
$V_p-\sigma_T-SSN-F10.7-V_A-S_p-T_{exp}/T_p$ Camporeale et al. [2017]	99.7	98.7	97.5	96.1	98.2
$V_p-\sigma_T-SSN-F10.7-V_A-S_p-T_{exp}/T_p$ KNN (this work)	99.6	95.2	88.5	93.0	94.9
$B_T-N_P-T_P-V_P-N_{ap}-T_{exp}/T_P-S_p-M_f$ KNN (this work)	99.2	91.1	83.8	92.9	92.8

S_p - T_{exp}/T_p scheme (σ_T is the standard deviation of proton temperature, SSN is the sunspot number, and $F10.7$ is the solar radio flux at 10.7 cm), they concluded that they have obtained “excellent” classification accuracies, which are better than 96% for all the four types of solar wind. Note that, 25% of the database is used for training in [Camporeale et al., 2017], but the ratio is 75% in our study. If the same parameter scheme was performed on KNN classifier, the overall classification accuracy has a slight decrease of 3.3%, although the accuracy for SRRP has a decrease of 9.0%, as listed in Table 4. This indicates that the performance of KNN classifier is close to, or not far worse than, that of Gaussian Process classifier used by Camporeale et al. [2017].

We apply the trained KNN classifier to classify the OMNI data set from 1963 to 2017. The probabilities of CHOP, SBP, SRRP, EJECT are obtained. As mentioned before, the threshold of probability is chosen to be 0.3-0.5 to obtain optimal TPR and FPR. The event with the maximum of probability less than the threshold is defined as an “undecided” event. If the threshold is chosen to be 0.3, the percentage of “undecided” events is 0.02%. And if the threshold is chosen to be 0.5, the percentage of “undecided” events is less than 2.2%. For comparison, the percentage of “undecided” events is 0.2% and 7.5% in Camporeale et al. [2017], indicating that the possibility of “undecided” solar wind type is larger than our approach.

4 Discussion

4.1 daily sampled parameters are not recommended for hourly solar wind classification

Camporeale et al. [2017] used the mixture of hourly averaged solar wind parameters and daily sampled parameters to obtain “excellent” classification accuracies, however, it is not recommended in this study. Firstly, the time resolution of SSN and $F10.7$ used by Camporeale et al. [2017] is one day, which does not match the temporal resolution of reference solar wind data sets and other five solar wind parameters, which are one hour. Camporeale et al. [2017] did not demonstrate the reasonableness of such an approach. Secondly, SSN and $F10.7$ are found to be questionable in solar wind classification. Taking the SSN - $F10.7$ scheme for example, the overall accuracy obtained by KNN classifier is 98.5%, and is 99.5%, 98.9%, 98.1%, and 96.6%, for CHOP, SBP, SRRP, and EJECT, respectively, which is even better than the results of Camporeale et al. [2017]. However, it does not indicate that SSN -

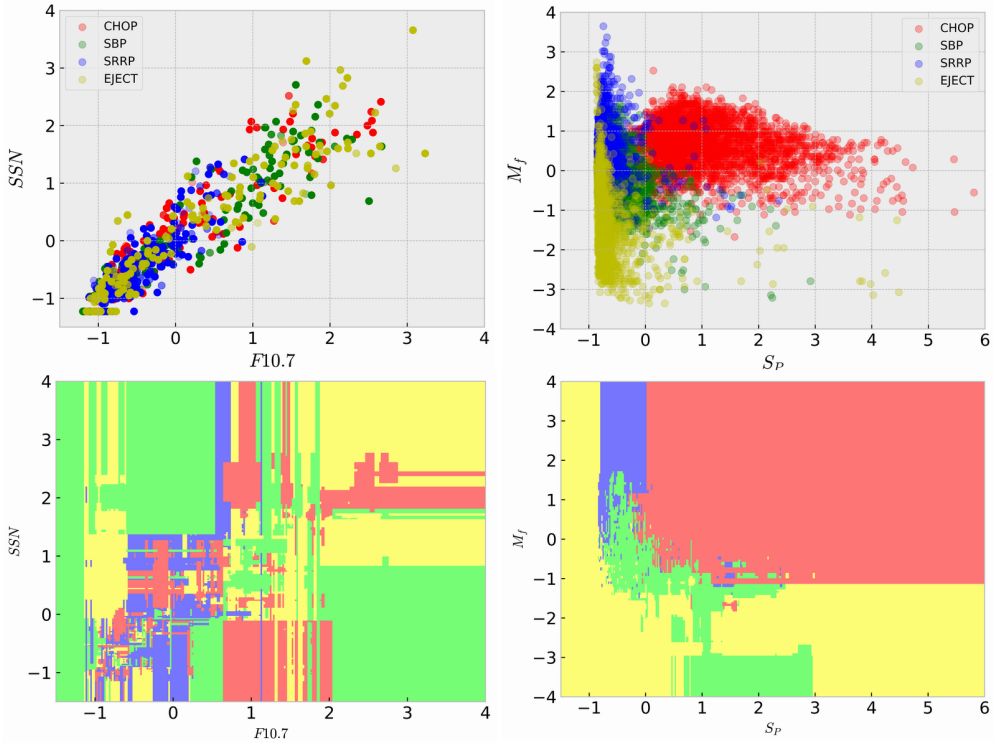


Figure 5. Top: Distribution of reference solar wind in the plot of SSN vs. $F10.7$ and M_f vs. S_p . Bottom: Corresponding decision boundaries for each solar wind category. The overall accuracy given by KNN classifier under the SSN - $F10.7$ scheme is 98.5%, however, the accuracy is 79.2% under the M_f - S_p scheme.

$F10.7$ scheme is a better choice in solar wind classification. As shown in Figure 5, it is quite difficult to distinguish CHOP, SBP, SRRP, and EJECT from each other in the plot of SSN vs. $F10.7$. At the same time, the corresponding decision boundaries for each solar wind category are too complicate to eliminate the concerns on the probability of over-fitting problem. One plausible reason is that there are only 479 independent data points in the plot of SSN vs. $F10.7$ for 8625 events. The ratio of independent data (< 6%) is much less than the ratio of training dataset (75% in our work and 10%-25% in Camporeale et al. [2017]), which means that all the independent data are used both for training and for testing. In other word, the cross validation does not work at all, which may result in a lager risk of over-fitting problem. For comparison, the distribution of reference solar wind in the plot of M_f vs. S_p is also shown in Figure 5. Although the overall accuracy given by KNN classifier is 79.2%, much lower than that for SSN - $F10.7$ scheme, it is still possible to generally distinguish the distribution of CHOP, SBP, SRRP, and EJECT from each other, except a few overlaps. And the decision boundaries are more likely to represent a regularized classification. Thirdly, Camporeale et al. [2017] did not explain that the classification performance significantly increases when using both SSN and $F10.7$ with respect to the case when one of the two is left out, although SSN and $F10.7$ are strongly correlated. Thus, it is strongly suggested to use the solar wind parameters with the same time resolutions as the reference solar wind data sets when training the classifier.

4.2 Composition information in solar wind classification

In the previous classification schemes in two- or three- dimensional parameter space, solar wind composition measurement indeed plays an important role in solar wind classification. However, it is still difficult to conclude that the composition measurement is thus indispensable. To show the importance of composition information in solar wind classification, we have accessed the 1-hr composition data ($C6+/C5+$, $O7+/O6+$) from ACE satellite during 1998-2011. During this time interval, the reference solar wind data sets with data gap removed are 8021 hours: CHOP (2881 hours), SBOP (2215 hours), SRRP (1694 hours), Ejecta (1231 hours). Compared to the data sets without composition information, the Ejecta data reduced from 1835 hours to 1231 hours, and the CHOP, SBOP, SRRP data are the same. The overall classification accuracy by solely using $C6+/C5+$ or $O7+/O6+$ is 51.0% and 65.9%, which is less or comparable to the performance, 66.7%, when S_p is used solely.

The comparison of classification results with/without composition information is shown in Table 5. It is clear that the classification results indeed have some minor improvements, especially when O^{7+}/O^{6+} information is considered. But the improvements are not much significant, only 1.5%. Considering that most of solar wind satellites, for example, the recent Parker Solar Probe, do not have composition instrument, it is suggested that solar wind classification scheme without composition information is still useful.

Table 5. Comparison of solar wind classification with/without composition information

	CHOP	SBP	SRRP	EJECT	4-type	HKSS
Without Composition	99.3	91.4	85.1	92.5	93.1	0.903
C^{6+}/C^{5+}	99.3	92.5	85.6	92.6	93.5	0.909
O^{7+}/O^{6+}	99.4	93.0	89.0	94.1	94.6	0.925
C^{6+}/C^{5+} & O^{7+}/O^{6+}	99.4	93.2	87.3	93.1	94.3	0.920

4.3 Importance of the accuracy of reference solar wind

The reference solar wind with known types is very important for supervised machine learning. In this study, the reference solar wind data comes from the work based on human experiences, which may have some uncertainties, especially at the boundaries of events. A natural thought is that the center part of an event has the highest probability to be correctly labeled. For practice, if 3-hr data points at both boundaries were deleted for each EJECT event, the classification accuracy of EJECT should have an improvement of 2.2%. Thus, the further improvement of classification accuracy by machine learning is limited by the uncertainties of the reference solar wind data set.

5 Application in Space Weather Early Warning

The information of solar wind origin may be helpful for the early warnings of space weather. Firstly, the solar wind category is useful for the risk evaluation of a predicted geomagnetic storm. Turner et al. [2009] showed that the storm intensity and occurrence rate of intense storm (Dst minimum < -100 nT) for ICME-driven storms are larger than that for CIR-driven storms. The average Dst minimum during a CIR-driven storm is ~ -74 nT, and the oc-

urrence rate of intense storms is only 13%, however, these two values are -128 nT and 57% for ICME-driven storms, respectively. Besides, all superstorms, with Dst minimum < -300 nT and midday magnetopause shifting earthward of geosynchronous orbit [Li et al., 2010], are associated with ICMEs. Secondly, the classification of CHOP and EJECT is also helpful for the risk evaluation of surface charging of geosynchronous spacecrafsts. [Borovsky & Denton, 2006; Denton et al., 1995] found that the magnitude of spacecraft potential is, on average, significantly elevated for CIR-driven storms than during ICME-driven storms. Thirdly, McGranaghan et al. [2014] showed that SBP and SRRP produce forecastable changes in thermospheric density.

Gonzalez & Tsurutani [1987] suggested that storm intensity depends on the intensity of southward interplanetary B_Z and the threshold for intense storms is summarized to be -10 nT. Echer et al. [2008] later found that storm intensity depends on the solar wind electric field E_Y and the threshold for intense storms is summarized to be 5 mV/m. If $B_Z \leq -10$ nT and $E_Y \geq 5$ mV/m are observed in the solar wind at L1 point, a magnetic storm is likely to occur in the next several hours. With the information of solar wind type obtained, more details of the geoeffectiveness will be inferred. Table 6 gives two examples. For the first case, B_Z is observed to be -11.2 nT on 00:00 Feb-27-2003, moreover, the corresponding E_Y is observed to be 5.03 mV/m. Based on our classification algorithm, the solar wind plasma is categorized to be SBP, indicating a possible CIR-driven storm. Borovsky & Denton [2013] indeed identified that event as a pseudostreamer CIR. Thus, the impending storm will be predicted to be a moderate storm with a big probability, at the same time, the risk of dangerous spacecraft surface charing is predicted to be high. As a validation, the real occurred storm is identified to be a moderate storm, with the Dst minimum of -60 nT. Besides, the magnitude of spacecraft potential (Φ) in geosynchronous orbit during this storm is close to 4000 V. For the second case, similar B_Z and E_Y are observed to be -10.8 nT and 5.08 mV/m on 00:00 Nov-08-1998. Unlike, the solar wind plasma is categorized to be EJECT for this case, (which is later identified as an ICME by Richardson and Cane later, <http://www.srl.caltech.edu/ACE/ASC/DATA/level3/icmetable2.htm>), indicating a possible ICME-driven storm. Thus, the impending storm will likely be an intense storm, however, the risk of spacecraft surface charging is predicted to be relative low. In fact, the following storm has an intensity of -149 nT and the magnitude of spacecraft potential during this storm is no more than 900 V.

Table 6. Application of the information of solar wind origin in improving space weather forecast.

Time	B_Z	E_Y	Type	Forecast	Dst_{min}	Φ^a
Feb-27-2003 00:00 UT	-11.2	5.03	SBP	Moderate CIR-storm high charging risk	-60	4000
Nov-08-1998 00:00 UT	-10.8	5.08	EJECT	Intense ICME-storm low charging risk	-149	900

^a Data from the LANL/MPA instrument.

At present, we use the in-situ observation at L1 point to classify the solar wind, and can make a space weather early warning by half an hour or more. There could be more utility for the present classification scheme if a solar wind monitor is placed at L5. Besides, we are still working on improving the time advance of solar wind classification by using the observations on the Sun's surface.

6 Summary

Solar wind categorization is conducive to understanding the solar wind origin and physical processes ongoing at the Sun. Facing a great deal of spacecraft observations, manual classification based on rich experiences is prohibitive in terms of time and is challenged. Automatic classification methods are quite needed. Recently, with rapid developments in the field of artificial intelligence, the classification by machine learning is becoming more and more popular and powerful in big-volume data analysis, and furthermore, its performance is improving as well.

In this study, 10 popular supervised machine learning models, k -nearest neighbors (KNN), linear support vector machines (LSVM), SVM with a kernel of Gaussian radial basis function (RBFSVM), Decision Trees (DT), Random Forests (RF), Adaptive Boosting (Adaboost), Neural Network (NN), Gaussian Naive Bayes (GNB), Quadratic Discriminant Analysis (QDA), and eXtreme Gradient Boosting (XGBoost), are used to classify the solar wind at 1 AU into four plasma types: coronal-hole-origin plasma, streamer-belt-origin plasma, sector-reversal-region plasma, and ejecta.

A total of 13 parameters, each with 1-hr temporal resolution, are used for training the classifiers and searching for the best variable scheme. These parameters are the magnetic field intensity B_T , the proton number density N_P , the proton temperature T_P , the solar wind speed V_P , the proton-specific entropy S_p , the Alfvén speed V_A , the ratio of velocity-dependent expected proton temperature and proton temperature T_{exp}/T_P , the number density ratio of proton and alpha $N_{\alpha p}$, the dynamic pressure P_d , the solar wind electric field E_y , the plasma beta value β , the Alfvén Mach number M_A , and the fast magneto-sonic Mach number M_f . Note that, all the parameters can be obtained or derived from the typical solar wind observations. No composition measurements are needed, allowing our algorithm to be applied to most solar wind spacecraft data.

By exhaustive enumeration, an eight-dimensional scheme ($B_T, N_P, T_P, V_P, N_{\alpha p}, T_{exp}/T_P, S_p$, and M_f) is found to obtain the highest classification accuracy among all the 8191 combinations of the above 13 parameters. Among the 10 popular classifiers, the KNN classifier obtains an accuracy of 92.8%. It significantly improves the accuracy by 9.6% over existing manual schemes. In addition, small-scale flux rope events may also be able to be identified based on our method, though further validation is needed. Besides, two application examples of solar wind classification are given, indicating that it is helpful for the risk evaluation of predicted magnetic storms and surface charging of geosynchronous spacecrafts.

This work emphasizes the classification technique itself rather than the science of the solar wind origin. In the future, with new solar wind types and corresponding ideal events are proposed in the community, our machine learning approach will be updated accordingly and more efforts are needed to bring up some new understandings to the science of the solar wind origin.

Acknowledgments

We thank the OMNI database for the use of solar wind data, which is accessible in ftp://spdf.gsfc.nasa.gov/pub/data/omni/low_res_omni/. We also thank the scikit-learn and XGBoost toolkits written in Python, which provide the classification classifiers used here and can be found in <https://scikit-learn.org/stable/install.html>. The reference solar wind data for training and testing used in this study, and the final classified solar wind can be accessed in <http://www.spaceweather.ac.cn/%7Ehli/research.html>. This work was supported by Strategic Priority Research Program of Chinese Academy of Sciences (Grant No. XDA17010301),

NNSFC grants 41874203, 41574169, 41574159, 41731070, Young Elite Scientists Sponsorship Program by CAST, 2016QNRC001, and grants from Chinese Academy of Sciences (QYZDJ-SSW-JSC028, XDA15052500). H. Li was also supported by the Youth Innovation Promotion Association of the Chinese Academy of Sciences, and in part by the Specialized Research Fund for State Key Laboratories of China.

References

Antiochos, S. K., Mikić, Z., Titov, V. S., Lionello, R., & Linker, J. A. (2011). A model for the sources of the slow solar wind. *The Astrophysical Journal*, 731(2), 112. <https://doi.org/10.1088/0004-637X/731/2/112>.

Antonucci, E., Abbo, L., & Dodero, M. A. (2005). Slow wind and magnetic topology in the solar minimum corona in 1996-1997. *Astronomy & Astrophysics*, 435(2), 699-711. <https://doi.org/10.1051/0004-6361:20047126>.

Arge, C. N., Odstrcil, D., Pizzo, V. J., & Mayer, L. R. (2003). *Improved Method for Specifying Solar Wind Speed Near the Sun*. Paper presented at the Solar Wind Ten, <https://doi.org/10.1063/1.1618574>.

Arya S., & Freeman J. W. (2012). Estimates of solar wind velocity gradients between 0.3 and 1 AU based on velocity probability distributions from Helios 1 at perihelion and aphelion. *Journal of Geophysical Research: Space Physics*, 96(A8), 14183-14187. <https://doi.org/10.1029/91JA01135>.

Asbridge, J. R., Bame S. J., Feldman W. C., & Montgomery M. D. (1976). Helium and hydrogen velocity differences in the solar wind. *Journal of Geophysical Research*, 81(16), 2719-2727. <https://doi.org/10.1029/JA081i016p02719>.

Bame, S. J., Asbridge, J. R., Feldman, W. C., & Gosling, J. T. (1977). Evidence for a structure-free state at high solar wind speeds. *Journal of Geophysical Research*, 82, 1487-1492. <https://doi.org/10.1029/JA082i010p01487>.

Borovsky, J. E., & Denton, M. H. (2006). Differences between CME-driven storms and CIR-driven storms. *Journal of Geophysical Research*, 111(A7). <https://doi.org/10.1029/2005JA011447>.

Borovsky J. E. (2008). Flux tube texture of the solar wind: Strands of the magnetic carpet at 1 AU? *Journal of Geophysical Research: Space Physics*, 113(A8). <https://doi.org/10.1029/2007JA012684>.

Borovsky, J. E. (2010). On the variations of the solar wind magnetic field about the Parker spiral direction. *Journal of Geophysical Research: Space Physics*, 115(A9), A09101. <https://doi.org/10.1029/2009JA015040>.

Borovsky, J. E. (2012). The velocity and magnetic field fluctuations of the solar wind at 1 AU: Statistical analysis of Fourier spectra and correlations with plasma properties. *Journal of Geophysical Research: Space Physics*, 117(A5), A05104. <https://doi.org/10.1029/2011JA017499>.

Borovsky, J. E., & Denton, M. H. (2013). The differences between storms driven by helmet streamer CIRs and storms driven by pseudostreamer CIRs. *Journal of Geophysical Research: Space Physics*, 118(9), 5506-5521. <https://doi.org/10.1002/jgra.50524>.

Borovsky, J. E., & Denton, M. H. (2014). Exploring the cross correlations and autocorrelations of the ULF indices and incorporating the ULF indices into the systems science of the solar wind-driven magnetosphere. *Journal of Geophysical Research: Space Physics*, 119(6), 4307-4334. <https://doi.org/10.1002/2014JA019876>.

Bothmer, V., & Schwenn, R. (1996). Signatures of fast CMEs in interplanetary space. *Advances in Space Research*, 17(4), 319-322. [https://doi.org/10.1016/0273-1177\(95\)00593-4](https://doi.org/10.1016/0273-1177(95)00593-4).

Breiman, L., Friedman, J. H., Olshen, R. A., Stone, C. J. (1984). Classification and regression trees. Monterey, CA: Wadsworth & Brooks/Cole Advanced Books & Software. ISBN 978-0-412-04841-8.

Buhmann, M. D. (2003), Radial Basis Functions: Theory and Implementations, *Cambridge University Press*, ISBN 978-0-521-63338-3.

Cady, F. (2017). Machine Learning Classification, in The Data Science Handbook, John Wiley & Sons, Inc., Hoboken, New Jersey. doi: 10.1002/9781119092919.ch8.

Camporeale, E., Carè, A., & Borovsky, J. E. (2017). Classification of Solar Wind With Machine Learning: SOLAR WIND CLASSIFICATION. *Journal of Geophysical Research: Space Physics*, 122(11), 10,910-10,920. <https://doi.org/10.1002/2017JA024383>.

Chen, T., & Guestrin, C. (2016). XGBoost: A Scalable Tree Boosting System. In Proceedings of the 22Nd ACM SIGKDD International Conference on Knowledge Discovery and Data Mining (pp. 785-794). New York, NY, USA: ACM. <https://doi.org/10.1145/2939672.2939785>

Crooker, N. U., Antiochos, S. K., Zhao, X., & Neugebauer, M. (2012). Global network of slow solar wind. *Journal of Geophysical Research: Space Physics*, 117(A4), A04104. <https://doi.org/10.1029/2011JA017236>.

Denoeux, T. (1995). A K-Nearest Neighbor Classification Rule-Based on Dempster-Shafer Theory. *IEEE Transactions on Systems Man and Cybernetics*, 25(5), 804-813. <https://doi.org/10.1109/21.376493>.

Denton, M. H., Borovsky, J. E., Skoug, R. M., Thomsen, M. F., Lavraud, B., Henderson, M. G., et al. (2006). Geomagnetic storms driven by ICME- and CIR-dominated solar wind. *Journal of Geophysical Research*, 111(A7). <https://doi.org/10.1029/2005JA011436>.

Echer, E., W. D. Gonzalez, B. T. Tsurutani, and A. L. C. Gonzalez (2008), Interplanetary Conditions Causing Intense Geomagnetic Storms ($Dst \leq -100$ nT) during solar cycle 23 (1996-2006), *J. Geophys. Res.*, 113, A05221, doi:10.1029/2007JA012744.

Eyni, M., & Steinitz, R. (1978). Cooling of slow solar wind protons from the HELIOS 1 experiment. *Journal of Geophysical Research*, 83, 4387. <https://doi.org/10.1029/JA083iA09p04387>.

Fan, R. E., Chang, K. W., Hsieh, C. J., Wang, X. R., Lin, C. J. (2008). LIBLINEAR: A library for large linear classification. *Journal of Machine Learning Research*. 9: 1871-1874.

Feldman, U., Landi, E., & Schwadron, N. A. (2005). On the sources of fast and slow solar wind. *Journal of Geophysical Research: Space Physics*, 110, A07109. <https://doi.org/10.1029/2004JA010918>.

Fisk, L. A., Zurbuchen, T. H., & Schwadron, N. A. (1999). On the coronal magnetic field: consequences of large-scale motions. *The Astrophysical Journal*, 521, 868-877. <https://doi.org/10.1086/307556>.

Foullon, C., Lavraud, B., Luhmann, J. G., Farrugia, C. J., Retinò, A., Simunac, K. D. C., et al. (2011). Plasmoid releases in the heliospheric current sheet and associated coronal hole boundary layer evolution. *The Astrophysical Journal*, 737(1), 16. <https://doi.org/10.1088/0004-637X/737/1/16>.

Gonzafcz, W. D. & Tsurutani, B. T., Criteria of interplanetary parameters causing intense magnetic storms ($Dst < -100$ nT), *Planet. Space Sci.*, 35, 1101, 1987.

Gosling, J. T., Borrini G., Asbridge J. R., Bame S. J., Feldman W. C., & Hansen R. T. (2012). Coronal streamers in the solar wind at 1 AU. *Journal of Geophysical Research: Space Physics*, 86(A7), 5438-5448. <https://doi.org/10.1029/JA086iA07p05438>.

Hellinger, P., Matteini, L., Štverák, Š., Trávníček, P. M., & Marsch, E. (2011). Heating and cooling of protons in the fast solar wind between 0.3 and 1 AU: Helios revisited. *Journal of Geophysical Research: Space Physics*, 116(A9), A09105. <https://doi.org/10.1029/2011JA016674>.

Ho, T. K. (1995). Random Decision Forests. Proceedings of the 3rd International Conference on Document Analysis and Recognition, Montreal, QC, 14-16 August 1995. pp. 278-282.

Jian, L., Russell, C. T., Luhmann, J. G., & Skoug, R. M. (2006). Properties of Interplanetary Coronal Mass Ejections at One AU During 1995-2004. *Solar Physics*, 239(1-2), 393-436. <https://doi.org/10.1007/s11207-006-0133-2>.

Klein, L. W., & Burlaga, L. F. (1982). Interplanetary magnetic clouds at 1 AU. *Journal of Geophysical Research*, 87, 613-624. <https://doi.org/10.1029/JA087iA02p00613>.

Kunow, H., Crooker, N. U., Linker, J. A., Schwenn, R., & Von Steiger, R. (Eds.). (2006). *Coronal mass ejections*. Dordrecht; Norwell, MA: Springer, 484.

Lepping, R. P., Wu, C.-C., & Berdichevsky, D. B. (2005). Automatic identification of magnetic clouds and cloud-like regions at 1 AU: occurrence rate and other properties. *Annales Geophysicae*, 23(7), 2687-2704. <https://doi.org/10.5194/angeo-23-2687-2005>.

Li, G., Miao, B., Hu, Q., & Qin, G. (2011). Effect of Current Sheets on the Solar Wind Magnetic Field Power Spectrum from the Ulysses Observation: From Kraichnan to Kolmogorov Scaling. *Physical Review Letters*, 106(12). <https://doi.org/10.1103/PhysRevLett.106.125001>.

Li, H., C. Wang, and J. R. Kan (2010), Midday magnetopause shifts earthward of geosynchronous orbit during geomagnetic superstorms with $Dst \leq -300$ nT, *J. Geophys. Res.*, 115, A08230, doi:10.1029/2009JA014612.

Li, H., Wang, C., He, J., Zhang, L., Richardson, J. D., Belcher, J. W., & Tu, C. (2016). Plasma heating inside interplanetary coronal mass ejections by Alfvénic fluctuations dissipation. *The Astrophysical Journal Letters*, 831(2), L13. <https://doi.org/10.3847/2041-8205/831/2/L13>.

Li, H., Wang, C., Richardson, J. D., & Tu, C. (2017). Evolution of Alfvénic Fluctuations inside an Interplanetary Coronal Mass Ejection and Their Contribution to Local Plasma Heating: Joint Observations from 1.0 to 5.4 au. *The Astrophysical Journal*, 851(1), L2. <https://doi.org/10.3847/2041-8213/aa9c3f>.

Luttrell, A. H., & Richter A. K. (1988). The role of Alfvénic fluctuations in MHD turbulence evolution between 0.3 and 1 AU, in Proceedings of the Sixth International Solar Wind Conference, NCAR TN-306, edited by V. J. Pizzo, T. E. Holzer, and D. G. Sime, 335 pp., Boulder, Colo.

Mariani, F., Bavassano, B., & Villante, U. (1983). A statistical study of MHD discontinuities in the inner solar system-HELIOS 1 and 2. *Solar Physics*, 83, 349-365.

<https://doi.org/10.1007/BF00148285>.

Marsch, E., Rosenbauer, H., Schwenn, R., Muehlhaeuser, K.-H., & Neubauer, F. M. (1982). Solar wind helium ions-Observations of the HELIOS solar probes between 0.3 and 1 AU. *Journal of Geophysical Research*, 87, 35-51. <https://doi.org/10.1029/JA087iA01p00035>.

Matthaeus, W. H., Breech, B., Dmitruk, P., Bemporad, A., Poletto, G., Velli, M., & Romoli, M. (2007). Density and Magnetic Field Signatures of Interplanetary 1/f Noise. *The Astrophysical Journal Letters*, 657(2), L121. <https://doi.org/10.1086/513075>.

McComas, D. J., Ebert, R. W., Elliott, H. A., Goldstein, B. E., Gosling, J. T., Schwadron, N. A., & Skoug, R. M. (2008). Weaker solar wind from the polar coronal holes and the whole Sun. *Geophysical Research Letters*, 35, L18103. <https://doi.org/10.1029/2008GL034896>.

McGranaghan, R., D. J. Knipp, R. L. McPherron, and L. A. Hunt (2014), Impact of equinoctial high-speed stream structures on thermospheric responses, *Space Weather*, 12, 277–297, doi:10.1002/2014SW001045.

Moldwin, M. B., Ford, S., Lepping, R., Slavin, J., & Szabo, A. (2000). Small-scale magnetic flux ropes in the solar wind. *Geophysical Research Letters*, 27(1), 57-60. <https://doi.org/10.1029/1999GL010724>.

Neugebauer, M., Steinberg, J. T., Tokar, R. L., Barraclough, B. L., Dors, E. E., & Wiens, R. C., et al. (2003). Genesis On-board Determination of the Solar Wind Flow Regime. In C. T. Russell (Ed.), *The Genesis Mission* (pp. 153-171). Dordrecht: Springer Netherlands. https://doi.org/10.1007/978-94-010-0241-7_6.

Pedregosa F, Varoquaux G, Gramfort A, Michel V, & Thirion B, et al. (2011). Scikit-learn: Machine learning in Python. *Journal of Machine Learning Research* 12: 2825-2830. doi: 10.3389/fninf.2014.00014.

Perez, A., Larranaga, P., & Inza, I. (2006). Supervised classification with conditional Gaussian networks: Increasing the structure complexity from naive Bayes. *International Journal of Approximate Reasoning*, 43(1), 1-25.

Reisenfeld, D. B., Steinberg, J. T., Barraclough, B. L., Dors, E. E., Wiens, R. C., & Neugebauer, M., et al. (2003). Comparison Of The Genesis Solar Wind Regime Algorithm Results With Solar Wind Composition Observed By ACE. *AIP Conference Proceedings*, 679(1), 632-635. <https://doi.org/10.1063/1.1618674>.

Richardson, I. G., Cliver, E. W., & Cane, H. V. (2000). Sources of geomagnetic activity over the solar cycle: Relative importance of coronal mass ejections, high-speed streams, and slow solar wind. *Journal of Geophysical Research*, 105, 18203-18213.

<https://doi.org/10.1029/1999JA000400>.

Richardson, I. G., & H. V. Cane (2004), The fraction of interplanetary coronal mass ejections that are magnetic clouds: Evidence for a solar cycle variation, *Geophysical Research Letters*, 31, L18804, doi:10.1029/2004GL020958.

Richardson, I. G., & Cane, H. V. (2010). Near-Earth Interplanetary Coronal Mass Ejections During Solar Cycle 23 (1996-2009) Catalog and Summary of Properties. *Solar Physics*, 264(1), 189-237. <https://doi.org/10.1007/s11207-010-9568-6>.

Rojas, R. (1996). Neural Networks-A Systematic Introduction, Springer-Verlag, Berlin, New-York.

Schwenn, R. (1990), Large scale structure of the interplanetary medium, in Physics of the Inner Heliosphere I, edited by R. Schwenn and E. Marsch, 99 pp., Springer, Berlin.

Schwenn, R. (2006). Solar Wind Sources and Their Variations Over the Solar Cycle. *Space Science Reviews*, 124(1-4), 51-76. <https://doi.org/10.1007/s11214-006-9099-5>.

Sheeley, N. R., Harvey, J. W., & Feldman, W. C. (1976). Coronal holes, solar wind streams, and recurrent geomagnetic disturbances: 1973-1976. *Solar Physics*, 49(2), 271-278. <https://doi.org/10.1007/BF00162451>.

Srivastava, S., Gupta, M. R., & Frigyik, B. A. (2007). Bayesian quadratic discriminant analysis. *Journal of Machine Learning Research*, 8, 1277-1305.

Subramanian, S., Madjarska, M. S., & Doyle, J. G. (2010). Coronal hole boundaries evolution at small scales: II. XRT view. Can small-scale outflows at CHBs be a source of the slow solar wind? *Astronomy and Astrophysics*, 516, A50. <https://doi.org/10.1051/0004-6361/200913624>.

Suess, S. T., Ko, Y.-K., von Steiger, R., & Moore, R. L. (2009). Quiescent current sheets in the solar wind and origins of slow wind. *Journal of Geophysical Research: Space Physics*, 114, A04103. <https://doi.org/10.1029/2008JA013704>.

Thieme, K. M., Schwenn, R., & Marsch, E. (1989). Are structures in high-speed streams signatures of coronal fine structures? *Advances in Space Research*, 9, 127-130. [https://doi.org/10.1016/0273-1177\(89\)90105-1](https://doi.org/10.1016/0273-1177(89)90105-1).

Thieme, K. M., Marsch, E., & Schwenn, R. (1990). Spatial structures in high-speed streams as signatures of fine structures in coronal holes. *Annales Geophysicae*, 8, 713-723.

Tu, C.-Y., & Marsch, E. (1995). MHD structures, waves and turbulence in the solar wind: Observations and theories. *Space Science Reviews*, 73(1-2), 1-210.

Turner, N. E., Cramer, W. D., Earles, S. K., & Emery, B. A. (2009). Geoefficiency and energy partitioning in CIR-driven and CME-driven storms. *Journal of Atmospheric and Solar-Terrestrial Physics*, 71(10-11), 1023-1031. <https://doi.org/10.1016/j.jastp.2009.02.005>.

von Steiger, R., Zurbuchen, T. H., & McComas, D. J. (2010). Oxygen flux in the solar wind: Ulysses observations. *Geophysical Research Letters*, 37(22), L22101. <https://doi.org/10.1029/2010GL045389>.

Wang, Y.-M., & Sheeley, N. R. (1990). Solar wind speed and coronal flux-tube expansion. *The Astrophysical Journal*, 355, 726-732. <https://doi.org/10.1086/168805>.

Xu, F., & Borovsky, J. E. (2015). A new four-plasma categorization scheme for the solar wind: 4-Plasma Solar-Wind Categorization. *Journal of Geophysical Research: Space Physics*, 120(1), 70-100. <https://doi.org/10.1002/2014JA020412>.

Yordanova, E., Balogh, A., Noullez, A., & von Steiger, R. (2009). Turbulence and intermittency in the heliospheric magnetic field in fast and slow solar wind: turbulence and intermittency in the solar wind. *Journal of Geophysical Research: Space Physics*, 114(A8), n/a-n/a. <https://doi.org/10.1029/2009JA014067>.

Zastenker, G. N., Koloskova, I. V., Riazantseva, M. O., Yurasov, A. S., Safrankova, J., & Nececk, Z., et al. (2014). Observation of fast variations of the helium-ion abundance in the solar wind. *Cosmic Research*, 52(1), 25-36. <https://doi.org/10.1134/S0010952514010109>.

Zhao, L., Zurbuchen, T. H., & Fisk, L. A. (2009). Global distribution of the solar wind during solar cycle 23: ACE observations. *Geophysical Research Letters*, 36(14). <https://doi.org/10.1029/2009GL039181>.

Zhu, J., Zou, H., Rosset, S. & Hastie, T. (2009). Multi-class adaboost. *Statistics and Its Interface*, 2, 349-360.

Zurbuchen, T. H., Fisk, L. A., Gloeckler, G., & von Steiger, R. (2002). The solar wind composition throughout the solar cycle: A continuum of dynamic states. *Geophysical Research Letters*, 29, 1352. <https://doi.org/10.1029/2001GL013946>.

Zurbuchen, T. H., & Richardson, I. G. (2006). In-Situ Solar Wind and Magnetic Field Signatures of Interplanetary Coronal Mass Ejections. *Space Science Reviews*, 123(1-3), 31-43. <https://doi.org/10.1007/s11214-006-9010-4>.